CHAPTER 21

Tailoring Colloidal Core–Shell Quantum Dots for Optoelectronics

ALI IMRAN CHANNA[a], YIMIN YOU[a], XIN TONG*[a,b]
AND ZHIMING M. WANG*[a]

[a]Institute of Fundamental and Frontier Sciences, University of Electronic Science and Technology of China, Chengdu 610054, PR China;
[b]Yangtze Delta Region Institute (Huzhou), University of Electronic Science and Technology of China, Huzhou 313001, PR China
*E-mail: xin.tong@uestc.edu.cn, zhmwang@uestc.edu.cn

21.1   Introduction

Colloidal quantum dots (QDs) are tiny crystals of semiconductor materials with dimensions in the nano-meter scale.[1] Owing to their small size, comparable to the exciton Bohr radius, QDs exhibit novel properties such as size-dependent optical band gaps for tunable absorption and emission spectra, which are very promising for various optoelectronic applications.[2,3] The small size also results in high surface-to-volume ratio of QDs,[4] and changes in surface conditions of QDs (such as oxygen, light, temperature *etc.*) may deteriorate their optical properties,[5] which is unfavorable for QDs-based optoelectronics.[6] Generally, during the synthesis of QDs, organic ligands from the solvent can assemble on their surface for passivation, keeping them stabilized and provide a monodispersed colloidal suspension of QDs.[7,8] However, the interaction between the QD and surface organic ligand is weak and during

Figure 21.1   Properties of bare QDs *versus* core–shell QDs.

the solution-processed fabrication of QDs-devices, the organic ligands may damage and provide insufficient protection to QDs against the surrounding environment, thus promoting the formation of new surface defects/traps.

The effective way to protect QDs' surface is to coat a secondary semiconductor shell on core QDs to form a core–shell structure. Figure 21.1 demonstrates the superior features of core–shell QDs compared to bare QDs, which exhibit enhanced optical properties and photo-/chemical stability against various environmental factors. More importantly, the size and composition of core and shell materials in core–shell QDs can be tailored to achieve various band alignments that suit different QDs-based optoelectronic applications, for example, high photoluminescence quantum yield (PLQY) and/ or efficient spatial charge separation. A suitable shell material can provide minimum lattice mismatch to core QDs and form proper band alignment to exhibit improved optical properties, which is essential for the growth of desirable core–shell QDs. A considerably large lattice mismatch between the core and shell may influence the properties of the core–shell due to strain effects. However, it is still feasible for the shell to form the crystal structure that matches with the core QDs during the growth process, thus minimizing the lattice mismatch for reduced interfacial defects.[9]

21.2   Classification of Core–Shell QDs

Colloidal core–shell QDs are generally categorized into type I, type II and quasi-type II on the basis of different band alignments between core and shell materials, as shown in Figure 21.2. The type I core–shell system consists of a
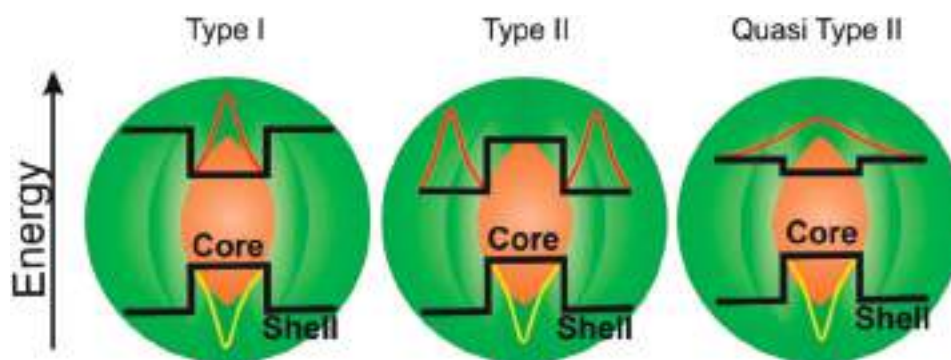
Figure 21.2   Schematic diagrams of type I, type II and quasi-type II band alignments for core–shell QDs.

shell with wider valence band (VB) and conduction band (CB) edges than the core, confining both the electrons and holes into the core region. This is beneficial to the radiative recombination of electrons and holes for enhanced PLQY and photo-stability. In the type II core–shell system, either the VB or CB edge of the shell resides within the bandgap of the core to form a staggered band alignment.[10] This type of core–shell structure exhibits long-lived recombination lifetimes of excitons owing to spatial separation of charge carriers (electrons and holes) upon excitation.[11,12]

In the quasi-type II core–shell structure, a small band offset exists between the CB or VB edges of core and shell, expanding the wave function of one type of carrier (generally for electrons) into both the core and shell region. Therefore, one type of charge carrier exists in the entire core–shell structure and the other type of carrier is confined in the core region.[13]

21.3   Synthesis and Optical Properties of Core–Shell QDs

Core–shell QDs can be synthesized either by one-step or two-step growth techniques. One-step growth techniques involve all the synthetic processes of core–shell QDs in the same pot.[14] Typically, after the growth of core QDs, the precursors for shell growth are directly injected into the core QDs reaction flask without stopping the reaction. While in a two-step growth technique, the core QDs are first grown and purified to remove the bulk and unreacted precursor. As-grown core QDs are then diluted in a suitable organic solvent for another reaction, in which the shell is grown at a suitable reaction temperature by injecting shell precursors.[9] Generally, all the semiconductors having smaller lattice mismatches with core are considered suitable materials for shell growth. In particular, shell thickness plays an important role in the optical properties of the core–shell QDs. An optimized shell thickness is required to realize efficient passivation for enhanced optical properties and improved charge transfer from QDs to other coupled semiconductor media.

21.3.1   Type I Core–Shell QDs

Type I core–shell structures (Figure 21.3a) have been developed to demonstrate enhanced PLQY and photo-/chemical stability. The examples of type I core–shell QDs include CdSe/ZnS, CdSe/ZnSe, CdS/ZnS,[15] InP/ZnS[16] and ZnSe/ZnS,[17] *etc.* Hines *et al.* have reported the growth of type I CdSe/ZnS core–shell QDs, in which a ZnS shell with a thickness of 1–2 monolayers was grown on CdSe core QDs.[18] The growth of the ZnS shell was carried out on pre-grown CdSe core QDs *via* sequentially injecting Zn and S shell precursors at a temperature of 300 °C.[18] The stock solutions for Zn and S were prepared by dissolving diethylzinc (Me_2Zn) and hexamethyldisilathiane [$S(TMS)_2$] into trioctylphosphine (TOP). Hao *et al.* also reported the synthesis of CdSe/ZnS core–shell QDs *via* a successive ionic layer adsorption and reaction (SILAR) technique.[19] The role of TOP solvent was highlighted for alleviating the strain effects during the growth of a thick ZnS shell, *i.e.* high-quality CdSe/ZnS core–shell QDs can be obtained by employing TOP solvent despite their higher lattice mismatch of ~10.6%.[20] Figure 21.3b,c exhibits the transmission electron microscope (TEM) images of CdSe core and CdSe/ZnS core–shell QDs, displaying controlled morphology and uniform particle size distribution.
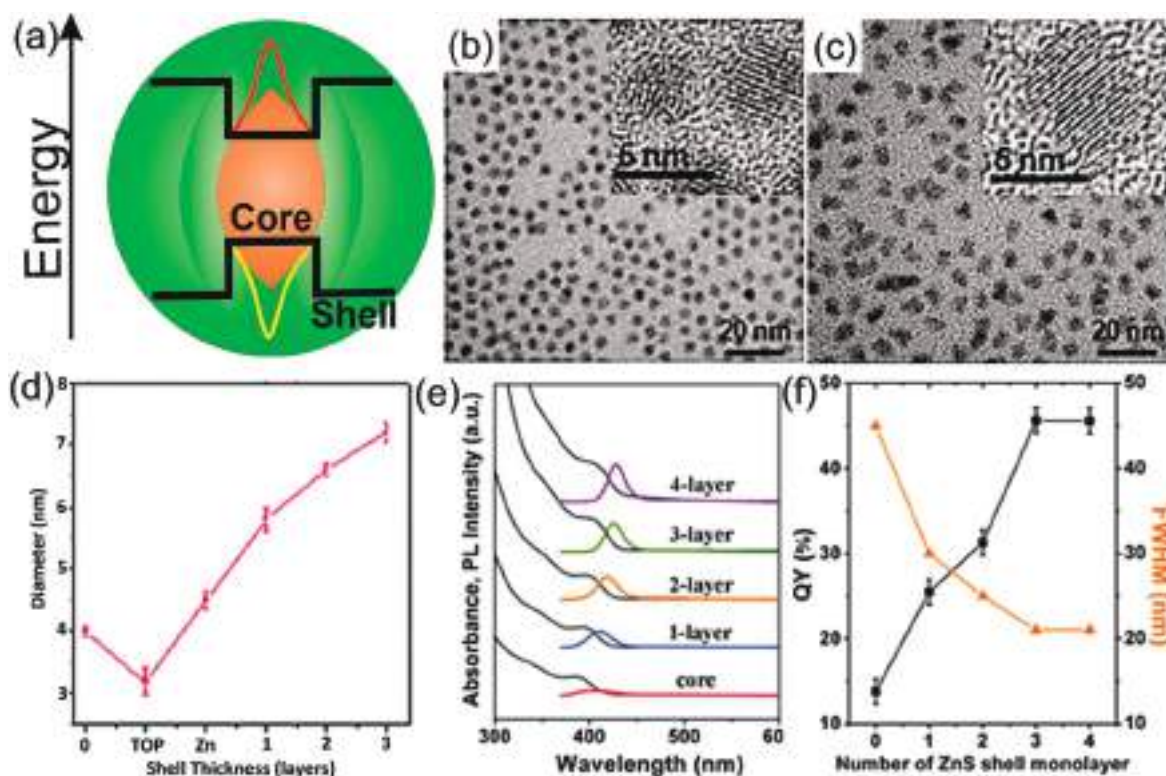

Figure 21.3   (a) Schematic diagram of type I core–shell structure. TEM images of (b) CdSe core and (c) CdSe/ZnS core–shell QDs. (d) Particle size *versus* shell thickness of CdSe/ZnS core–shell QDs. Adapted from ref. 19 with permission from the Royal Society of Chemistry. (e) Absorption and emission spectra of type I ZnSe/ZnS core–shell QDs. (f) QYs and FWHM of ZnSe/ZnS core–shell QDs with variable ZnS shell thickness. Adapted from ref. 21 with permission from the Royal Society of Chemistry.

A quick indication for the successful growth of shell on core QDs is the increasing average sizes of the QDs after the shell growth, as shown in Figure 21.3d. The decreased size of the CdSe core QDs after the introduction of TOP solvent was ascribed to the etching of CdSe core by the removal of excess Se from the surface *via* TOP.[19]

Low-temperature growth is often used to attain fine control on the particle size as well as to avoid the diffusion of shell material into core QDs. Bawendi *et al.* developed a low-temperature (140–220 °C) growth technique for the synthesis of CdSe/ZnS core–shell QDs.[22] Weller *et al.* used hexadecylamine (HDA) into trioctylphosphine oxide (TOPO)/TOP to tune particle size distribution.[23] Kudera *et al.* tailored the optical properties of CdSe/ZnS core–shell QDs to attain blue emission by lowering the particle size of QDs *via* using low growth temperature (80 °C).[24] The decreased particle size can lead to a strong quantum confinement effect in QDs, thus exhibiting enlarged band gaps for blue emission.

In type I core–shell QDs, the shell can passivate the defects and improve the original optical properties of the core QDs.[16,18] Figure 21.3e presents the ZnS shell thickness-dependent absorption and emission spectra of type I CdSe/ZnS core–shell QDs. The PL spectrum of CdSe core QDs exhibits a weak emission which showed considerable improvement (increased intensity) with increasing ZnS shell thickness, as shown in Figure 21.3e.[21] The increased ZnS shell also resulted in the enhanced PLQY (Figure 21.3f), that is, as-synthesized CdSe/ZnS core–shell QDs demonstrated suppressed surface defects and exhibited improved PLQY from 10% (bare CdSe QDs) to over 40%.[25]

21.3.2   Type II Core–Shell QDs

Bawendi *et al.* have developed type II core–shell QDs such as CdTe/CdSe and CdSe/ZnTe core–shell QDs.[11] As an example, CdTe/CdSe core–shell QDs were synthesized using CdO and TOP-Te precursors for the growth of CdTe core and CdO and TOP-Se for the growth of CdSe shell, respectively.[26] Wang *et al.* reported the synthesis of CdSe shell on CdTe core QDs *via* SILAR technique.[27] The CdTe core QDs mixed with TOP, tetradecylphosphonic acid (TDPA), and ODE were loaded into a round-bottom flask. The flask was heated at 170 °C after degassing and purging in an argon atmosphere. Cd and Se precursor solutions with equal molarity ratios were added alternately into the reaction flask at 30 min intervals. This technique yielded high-quality and homogenous CdTe/CdSe core–shell QDs, as depicted in Figure 21.4b,c. Xie and co-workers developed a variety of core–shell QDs employing ZnTe QDs as cores and CdTe, CdSe, CdS as shells.[28] The stock solutions for shell growth were prepared by dissolving cadmium oleate, TOP-Te, TOP-Se, and sulfur in 1-octadecane (ODE). The core–shell QDs were then obtained by injecting shell precursors into ZnTe core QDs, the variation in the morphology by lowering the shell growth temperature has been observed.[29,30] Highly luminescent type II CdS/ZnSe core–shell QDs were developed by Klimov's group.[31] The CdS core QDs were synthesized and dispersed in octadecylamine and
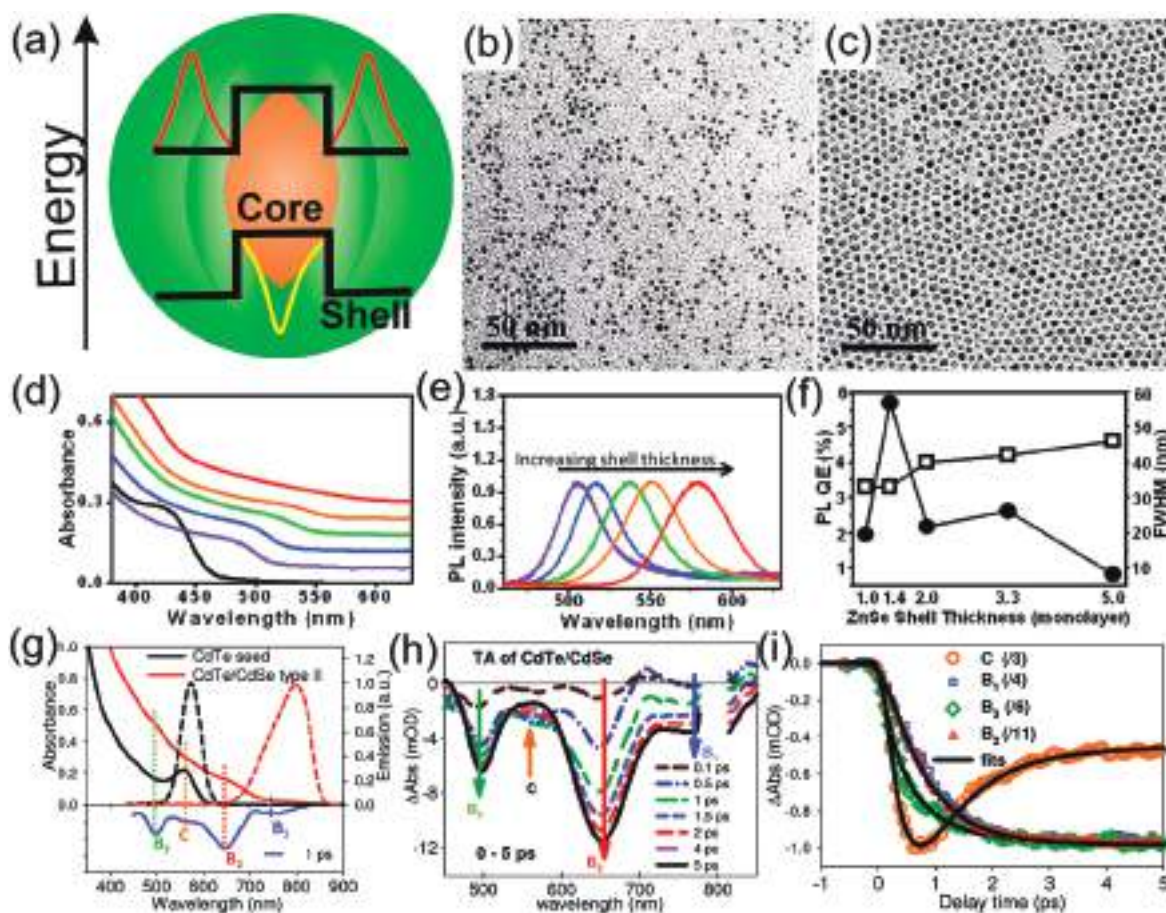
Figure 21.4 (a) Schematic diagram of type II core–shell QDs. TEM images of (b) CdTe core QDs and (c) CdTe/CdSe core–shell QDs. Adapted from ref. 27 with permission from American Chemical Society, Copyright 2013. (d) Absorption and (e) emission spectra of type II ZnTe/ZnSe core–shell QDs with increasing ZnSe shell thickness (black curve belongs to bare ZnTe QDs). (f) PLQE spectrum (circles) and FWHM trend (squares) for ZnTe/ZnSe core–shell QDs with variable ZnSe shell thickness. Adapted from ref. 33 with permission from American Chemical Society, Copyright 2010. (g) Absorption and emission spectra of CdTe core and CdTe/CdSe core–shell QDs. (h) TA spectra of CdTe/CdSe core–shell QDs. (i) Transient decay kinetics of transitions indicated in (h). Adapted from ref. 12 with permission from American Chemical Society, Copyright 2011.

ODE. Afterwards, ZnSe shell was grown by injecting zinc oleate and TOP-Se shell precursors into core QDs solution. Smith and co-workers have synthesized type II core–shell QDs with the existence of lattice strain.[32] Different shells with huge lattice mismatch (*e.g.* ZnS, ZnSe, ZnTe, CdS and CdSe) were grown on CdTe core QDs and as-prepared core–shell QDs exhibited a transition from type I to type II band structure.[32]

In contrast to the type I core–shell QDs, the optical properties of the type II core–shell QDs can exhibit red-shifted absorption and emission spectra with respect to the core QDs.[33] Figure 21.4d and e show the absorption and emission spectra of ZnTe core and ZnTe/ZnSe core–shell QDs with tunable optical properties by varying the shell thickness indicating a type II nature.

Figure 21.4f shows the shell thickness-dependent PL quantum efficiency (QE) and full width at half maxima (FWHM) of PL peaks. Over the course of ZnSe passivation the PLQE initially increased due to reduced surface defects and reached a PLQE of 6%. Further increase in ZnSe shell thickness leads to decreased PLQE due to enhanced type II spatial separation of electrons and holes.[11] The PL peak broadness showed gradual consistent increase with increasing shell thickness (Figure 21.4f). In type II core–shell QDs, the particle size inhomogeneity is defined as the convolution of core size and shell thickness distributions, which makes the PL bandwidth sensitive to the shell thickness.[33] CdTe/CdSe core–shell QDs also exhibited absorption spectrum extended to near-infrared (NIR) region compared to CdTe core QDs. Likewise, the emission spectrum of CdTe/CdSe core–shell QDs was red-shifted as compared to the CdTe core QDs due to the existence of type II band alignment (Figure 21.4g).[12]

The results indicated that tunable optical properties can be achieved by varying the shell thickness in type II core–shell QDs.[11,34] Moreover, the type II core–shell structures involve the transition of charge carriers between core and shell materials owing to the staggered band alignment. Figure 21.4g shows the absorption and emission spectra of CdTe/CdSe core–shell QDs with four absorption bands labeled as B1, B2, B3, and C at 770, 650, 500, and 560 nm, respectively (blue line spectrum in Figure 21.4g). These bands are more clearly observable in the transient absorption (TA) spectrum (Figure 21.4h) exhibiting bleaches at these bands due to the filling of CB electron levels.[12] The formation of bleach at the C band and its subsequent decay gives birth to the bleach signals of B1, B2, and B3 transitions. These transitions showed electron transfer from the CdTe (core) to CdSe (shell) CB. Moreover, B1, B2, and B3 transitions demonstrated identical bleach formation processes and decay kinetics, inferring that these transitions involve the same 1s electron level in the CdSe shell. This leads to the existence of an electron and hole in different regions of the core–shell structure, such as electrons in the shell and holes in the core, as exhibited by the bleach formation at B1, B2, and B3 (Figure 21.4h and i).[35–37] In this manner, the type II core–shell QDs exhibit prolonged PL lifetime with respect to the bare core QDs.[35]

21.3.3   Quasi-type II Core–Shell QDs

A typical quasi-type II band alignment (Figure 21.5a) is formed due to the small offset between CB and large offset between VB of the core and shell materials. In this way, the holes are localized in the core region and electrons are localized in both core and shell regions.[38] Various core–shell QDs have been developed with quasi-type II band alignment such as $CuInS_2$/CdS,[39] InP/CdS,[40] CdSe/CdS,[41] CdSe/ZnSe,[42] PbSe/CdSe,[43] $CuInSe_2$/$CuInS_2$,[44] $CuInSe_xS_{2−x}$/CdSeS/CdS[45] *etc.* CdSe/CdS core–shell QDs are interesting and among widely investigated quasi-type II core–shell systems due to their transition from type I to quasi-type II *via* tuning CdSe core size or CdS
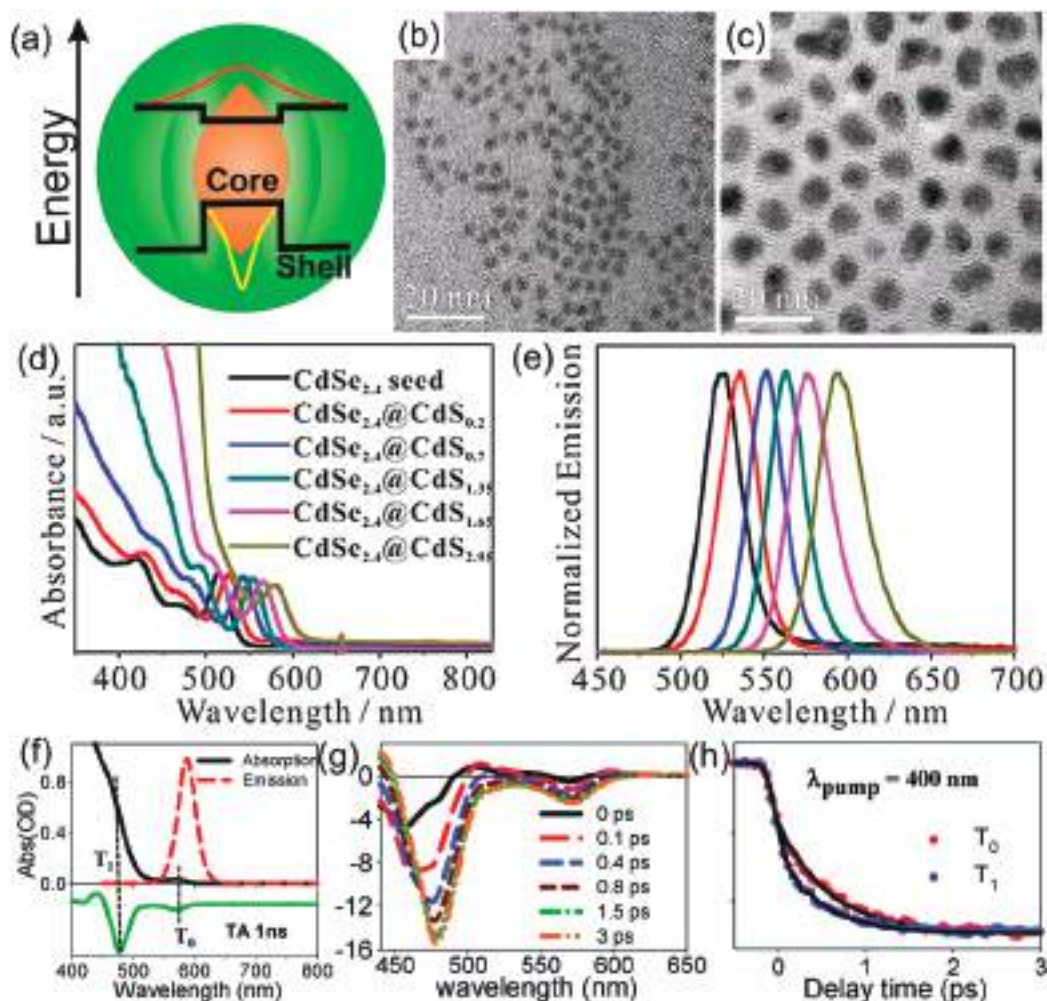
Figure 21.5 (a) Schematic diagram of quasi-type II core–shell structure. Representative TEM images of (b) CdSe core (c) CdSe/CdS (shell thickness ~2.95 nm) core–shell QDs. Absorption and emission spectra of (d) CdSe core and (e) CdSe/CdS core–shell QDs with variable shell thicknesses. Adapted from ref. 48 with permission from American Chemical Society, Copyright 2018. (f) Absorption and emission spectra with transient absorption spectrum (at 1 ns, green line) spectra of CdSe/CdS core–shell QDs. (g) TA spectra and (h) bleach formation kinetics CdSe/CdS QDs at indicated delay times. Adapted from ref. 50 with permission from American Chemical Society, Copyright 2012.

shell thickness.[46–48] Kong *et al.* have reported the synthesis of CdSe/CdS core–shell QDs in which the core QDs were synthesized *via* a hot injection approach.[48] CdS shell was grown on these CdSe core QDs by using SILAR process.[49] For this synthesis, cadmium precursor was prepared in advance by dissolving the calculated amount of CdO in oleylamine (OLA) and ODE at 300 °C and sulfur solution was prepared by dissolving sulfur in ODE *via* sonication. The shell precursor was then injected into core QDs at 200 °C after conventional degassing process. The core–shell QDs were further heated at 230 °C for improved crystallinity. Figure 21.5b and c show the

TEM images of CdSe core and CdSe/CdS core–shell QDs with CdS shell thickness of 2.95 nm, which is much obvious from the apparently large size of core–shell QDs compared to core QDs.

Figure 21.5d and e exhibit the absorption and emission spectra of CdSe core and CdSe/CdS core–shell QDs with variable shell thicknesses, which demonstrate the consistent red shifting of the first excitonic peak in absorption spectra and PL peaks.[48] In quasi-type II core–shell QDs, the FWHM of PL peaks with variable shell thickness showed no significant change as compared to that of the type II core–shell QDs, which indicates that the peak broadness is not sensitive to the shell thickness inhomogeneity (Figures 21.4e and 21.5e).

Figure 21.5f presents the absorption spectrum of CdSe/CdS core–shell QDs with a weak excitonic peak at ~575 nm (denoted as T_0) and strong absorption band at ~475 nm (denoted as T_1), which are clearer in TA spectrum (green line spectrum in Figure 21.5f). The T_0 band originated from the transition between the CB electron ($1s_e$) and VB hole ($1s_h$) levels in the core–shell structure. In the TA spectrum, the bleaches at T_1 and T_0 transitions exhibit identical $1s_e$ levels. The T_1 band hence appeared due to the transition between the delocalized $1s_e$ CB level and the VB edge level ($1s_h$) of the CdS shell.[50] After excitation *via* 400 nm laser, hot electrons and holes are generated at CB and VB edges. The relaxation of these excited hot carriers to the $1s_e$ and $1s_h$ levels leads to the continuous red-shift of the T_1 bleach and growth of T_0 bleach with a long lifetime, as shown in Figure 21.5g,h.[50]

21.4   Applications of Core–Shell QDs

Core–shell QDs offer a variety of applications owing to their excellent features compared to the bare QDs including engineered band structure, tunable optical properties (such as higher PLQY, narrow-band emission, and prolonged exciton lifetime), and robust photo-/chemical stability. Moreover, the facile and flexible solution-processed device fabrication steps make them highly desirable in optoelectronics. Herein, we present various core–shell QDs-based optoelectronic applications including solar cells, photoelectrochemical (PEC) cells, luminescent solar concentrators (LSCs), photodetectors, light emitting diodes (LEDs) and lasers.

21.4.1   Solar Cells

A solar cell is a photovoltaic (PV) device that converts solar energy into electricity. A typical QD-sensitized solar cell (QDSC) consists of three main elements including a photoanode, a counter electrode and electrolyte, as shown in Figure 21.6a.[51] Specifically, the photoanode is fabricated by using QDs as light absorbers and a wide band gap semiconductor (*e.g.* TiO_2 deposited on fluorine-doped tin oxide or indium-doped tin oxide glass) for electrons
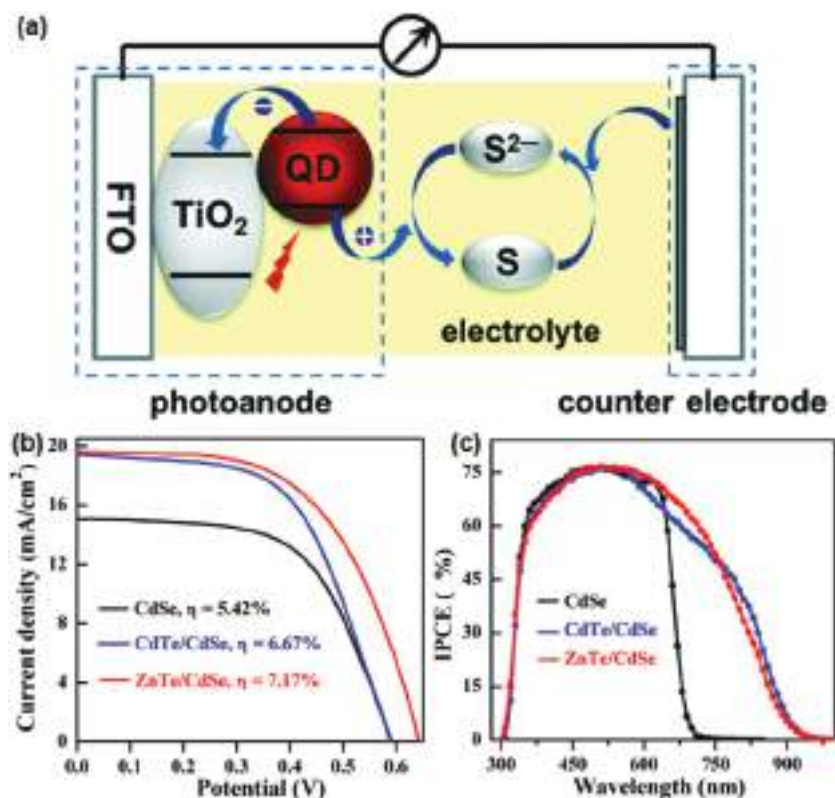
Figure 21.6 (a) Schematic diagram of a typical QD-sensitized solar cell. Adapted from ref. 51 with permission from the Royal Society of Chemistry. PV performance of bare CdSe QDs, CdTe/CdSe and ZnTe/CdSe core–shell QDs-based QDSCs: (b) J-V curves (c) IPCE curves. Adapted from ref. 52 with permission from American Chemical Society, Copyright 2015.

extraction. In this configuration, the photogenerated electrons in CB of QDs can be subsequently transferred to CB of TiO_2, FTO and the counter electrode.[51]

CdSe/ZnS core–shell QDs have been employed for the fabrication of QDSC and exhibited significantly enhanced stability compared to the bare CdSe QDs-based QDSC.[17] Ågren *et al.* synthesized ZnSe/CdS core–shell QDs for assembly of QDSC, yielding higher incident photon to current conversion efficiency (IPCE) due to efficient electron–hole separation derived from type II band structure.[53] Type II CdTe/CdS and CdTe/CdSeS core–shell QDs were also sensitized into TiO_2-based photoelectrode to fabricate the QDSCs, which demonstrated a power conversion efficiency (PCE) of 5.96% and 6.6%, respectively, under 1 sun illumination. The PCEs of core–shell QDs-based QDSCs are much higher than that of the CdTe core QDs-based QDSC (4.87%).[54] Such enhanced performance was ascribed to the extended absorption spectra and suppressed charge recombination of type II CdTe/CdS and CdTe/CdSeS core–shell QDs compared to the CdTe core QDs. Meng *et al.* employed $CdSe_xTe_{1-x}$/CdS core–shell QDs for the solar cell fabrication and reported a higher PCE than that of the bare $CdSe_xTe_{1-x}$ QDs with poor chemical stability.[55] A higher

PCE of 6.76% was obtained from CdTe/CdSe core–shell QDs-based QDSCs as compared to bare CdTe QDs, which was attributed to the broad light absorption of CdTe/CdSe core–shell QDs.[27] CdSeTe/CdS core–shell QDs were developed for the fabrication of QDSCs, as compared to the bare CdSeTe QDs-based device, the core–shell QDs-based device demonstrated a much higher PCE of 9.48% due to the suppressed surface defects by CdS shell passivation.[56]

QDSCs often suffer from low performance due to lower V_{oc} values, which suggests that increasing the V_{oc} is a prerequisite for further improvement in QDSC performance. In this regard, Bisquert *et al.* reported the synthesis of high-quality ZnTe/CdSe core–shell QDs with absorption in NIR region.[52] As-fabricated QDSCs exhibited a PCE of 7.17% and a certified efficiency of 6.82% under one sun illumination. The *J–V* curves and IPCE results for bare CdSe, CdTe/CdSe core–shell and ZnTe/CdSe core–shell QDs-based solar cells are displayed in Figure 21.6b and c, demonstrating PCEs of 5.43%, 6.67% and 7.17%, respectively. In addition, the V_{oc} values for these QDSCs are listed as 0.595 V, 0.597 V and 0.642 V, respectively. In these core–shell QDSCs, there exists a larger CB offset of ZnTe/CdSe core–shell QDs-TiO$_2$ (~1.22 eV) as compared to CdTe/CdSe core–shell QDs-TiO$_2$ (~0.27 eV), thus causing charge accumulation at QDs/TiO$_2$ interface and producing strong dipole effect.[57] This dipole effect delivered an upward shift of the TiO$_2$ CB, enabling higher performance in ZnTe/CdSe core–shell QDs-based QDSC than that of the CdTe/CdSe core–shell QDs.[58]

21.4.2   Photoelectrochemical Cells

A PEC cell is a water splitting system that enables the H$_2$ generation by utilizing solar energy, which mainly consists of a working electrode, a reference electrode and a counter electrode (Figure 21.7a). The working electrode is basically a photoelectrode made up of light sensitive semiconductor materials (such as QDs) which can generate electron–hole pairs upon exposure to sunlight.[59] QDs-based PEC cells have become a hot topic owing to the high absorption coefficient, multiple exciton generation and tunable optical properties of QDs, especially the core–shell QDs that demonstrate shell-engineered optical properties and improved photo-/chemical stability compared to bare QDs. Figure 21.7a illustrates the basic operation principle of a QD-PEC cell. After illumination by sunlight, electron–hole pairs are generated in the QDs. The electrons are transferred to the counter electrode by the applied external electric field where they take part in the targeted reaction such as water reduction reaction for hydrogen production whereas holes are consumed by the scavengers present in electrolyte.[9,44]

The bare QDs generally possess abundant surface defects and demonstrate poor PEC performance[44,45] Jin *et al.* have reported the synthesis of PbS/CdS core–shell QDs *via* cation exchange method for the fabrication of QDs-based PEC cells.[60] The PbS/CdS core–shell QDs decorated TiO$_2$ photoelectrode with further CdS SILAR coating exhibited a photocurrent density of ~11 mA cm^{-2} with decent stability.[60]
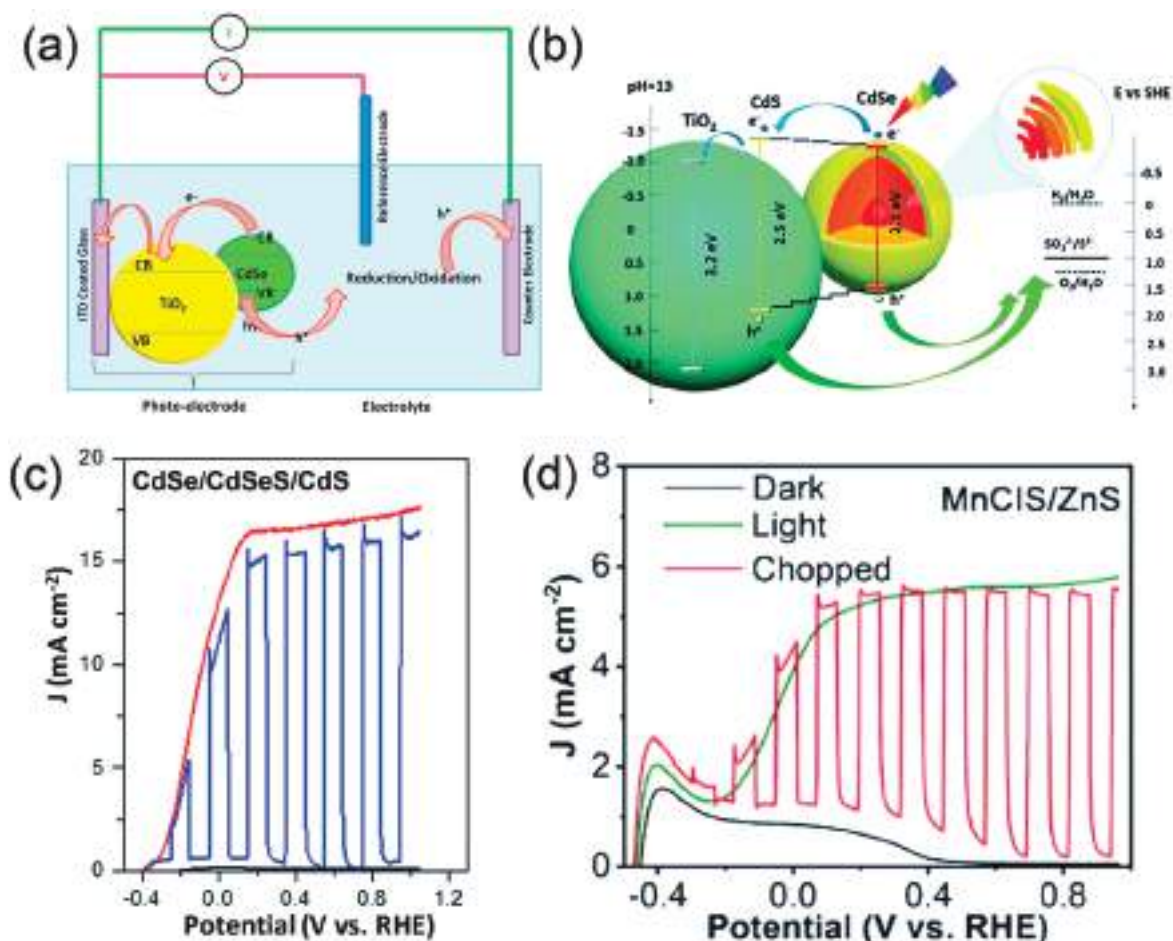
Figure 21.7 (a) Schematic illustration of a typical QDs/TiO$_2$-based PEC cell. Adapted from ref. 59 with permission from Elsevier, Copyright 2017. (b) Schematic diagram of the band structure and carrier transition of the CdSe/CdSeS/CdS core-alloyed–shell-shell QDs-based photoanode and corresponding (c) PEC performance. Adapted from ref. 61 with permission from the Royal Society of Chemistry. (d) PEC performance of heavy metal-free MnCIS/ZnS core–shell QDs-based photoanode. Adapted from ref. 62 with permission from the Royal Society of Chemistry.

Channa *et al.* developed CuGaS$_2$/CdS core–shell QDs for the fabrication of PEC photoelectrodes, which exhibited a higher photocurrent density of ~6.5 mA cm^{-2} than that of the CuGaS$_2$ core QDs (~0.83 mA cm^{-2}) under standard one sun illumination.[9] The higher performance in their case was ascribed to the enhanced absorption and prolonged exciton lifetime of the CuGaS$_2$/CdS core–shell QDs compared to bare CGS QDs. Wang *et al.* proposed and synthesized a novel type of interfacial engineered CdSe/CdSeS/CdS core–shell QDs with gradient CdSeS shell to establish stepped band alignment with optimized charge dynamics (Figure 21.7b) for obtaining high-performance PEC cells.[61] Figure 21.7c represents the PEC performance of the CdSe/CdSeS/CdS core/multi-shell QDs-based photoelectrode, which demonstrated a

maximum photocurrent density of 17.5 mA cm^{-2} under one sun illumination (AM 1.5 G, 100 mW cm^{-2}) with a retention of 70% photocurrent density after 2 hours.

However, despite the high efficiency of devices, the utilization of toxic heavy metals (*i.e.*, Pb, Cd *etc.*) based QDs for the application in PEC cells are deleterious for the environment and to human health. Environmentally friendly core–shell QDs are therefore highly demanded for practical applications. In this regard, Tong *et al.* reported pioneer work for the synthesis of heavy metal-free CuInSeS/ZnS core–shell QDs for the fabrication of heavy metal-free QDs-PEC cells.[63] The bare CuInSeS QDs-based photoelectrode only unveiled a photocurrent density of ~2.57 mA cm^{-2}. On the contrary, the CuInSeS/ZnS core–shell QD-incorporated photoelectrode revealed a significantly increased photocurrent density of ~4.3 mA cm^{-2} with retention of about ~77% photocurrent density after 2 hours. The enhanced performance of CuInSeS/ZnS core–shell QDs-based photoelectrode is attributed to the effective surface passivation of CuInSeS core QDs by ZnS shell, which leads to the suppressed non-radiative recombination and enhanced photo-/chemical stability, thus exhibiting much higher photocurrent density and enhanced device stability. Wang's group recently developed a heavy metal-free Mn-alloyed CuInS$_2$/ZnS core–shell QDs for the fabrication of environment friendly PEC cell.[62] Such Mn–CuInS$_2$/ZnS core–shell QDs-based PEC cell showed a photocurrent density as high as 5.7 mA cm^{-2} (Figure 21.7d) with outstanding retention of 73% of initial photocurrent density after 2 hours illumination. It was unveiled that the Mn-alloyed CuInS$_2$ core QDs possessed a larger band gap than the unalloyed CuInS$_2$, which formed a favorable band alignment (*i.e.* smaller conduction band offset) with ZnS shell for electron delocalization, which leads to efficient spatial charge separation of such core–shell QDs, thus consequently resulting in enhanced PEC performance. In addition, the ZnS shell can effectively protect the core QDs for improved photo-/chemical stability, giving rise to the excellent device durability.[62]

21.4.3   Luminescent Solar Concentrators

Luminescent solar concentrators (LSCs) have gained much interest for indoor building integrated PVs.[64–66] The motivation behind the fabrication of LSCs is to collect and concentrate solar radiation for application in low cost and high-performance PVs.[67,68] QDs-based LSCs are designed by embedding fluorescent QDs in transparent or semi-transparent materials (such as glass or polymer) as waveguide.[69,70] The incident light can be absorbed by the LSC and re-emitted/propagated to the waveguide edges *via* total internal reflection (TIR). The PV cells are attached to the lateral edges of the waveguide which collect the re-emitted light and convert it into electricity, as depicted in Figure 21.8.[71] Highly luminescent materials are very promising for the fabrication of LSCs such as organic dyes with high PLQY have been used as fluorophores for the fabrication of LSCs.[72] However, the poor photo-/chemical
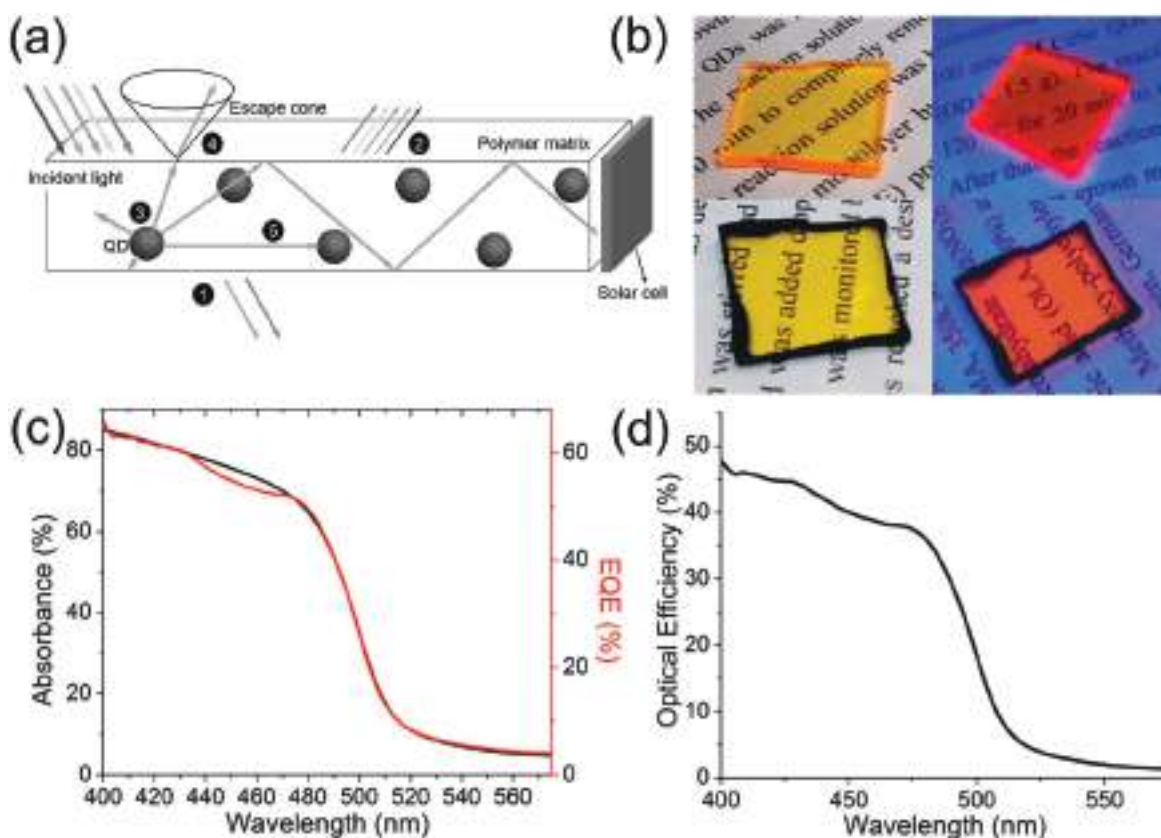
Figure 21.8 (a) Schematic diagram of a QDs-based LSC. Adapted from ref. 71 with permission from John Wiley & Sons, Copyright © 2016 WILEY-VCH Verlag GmbH & Co. KGaA, Weinheim. (b) CdSe/CdS core–shell QDs-based LSCs under ambient light (left panel) and UV light (right panel) with the edges clear (top) and blocked by carbon paint (bottom). (c) EQE spectrum of the prototype LSC. (d) Optical efficiency of the LSC. Adapted from ref. 79 with permission from American Chemical Society, Copyright 2014.

stability and overlapped absorption and emission spectra of such organic dyes limit the performance of corresponding LSCs.[73,74] Higher Stokes shift (difference in the energy between first exciton peak in the absorption spectrum and emission peak) is an important factor to realize high efficiency LSCs owing to reduced re-absorption losses. Colloidal core–shell QDs exhibit higher PLQY, shell thickness-dependent Stokes shift and improved photo-/chemical stability compared to organic dyes and bare QDs.[75,76] Numerous core–shell QDs, such as PbS/CdS, CdSe/CdS and CuInS$_2$/ZnS core–shell QDs have been employed for the fabrication of LSCs. Zhou *et al.* have reported NIR PbS/CdS core–shell QDs-based LSC.[77] They tuned the absorption and emission spectra by varying the size of the core and tailoring the thickness of the shell to exhibit large Stokes shift and higher PLQY.[77,78] Such PbS/CdS core–shell QDs with high PLQY and large Stokes shift can significantly reduce re-absorption losses for high efficiency, large-area LSCs. Furthermore, the PbS/CdS core–shell QDs-based LSC exhibited an optical efficiency (η_{opt}) of 6.1%,

which is much higher than that of bare PbS QDs-based LSC.[77] Bawendi *et al.* have developed LSCs from CdSe/CdS core–shell QDs with thick CdS shell (Figure 21.8b), demonstrating a very high QY of 86%.[79]

The EQE and absorbance spectra of LSC were in excellent agreement due to the minimal energy dependence of the QY (Figure 21.8c). The LSC fabricated using CdSe/CdS core–shell QDs exhibited an optical efficiency of 48% at a wavelength of 400 nm due to a higher magnitude of absorption at 400 nm (Figure 21.8d). However, at longer wavelengths, there is a reduction in the LSCs optical efficiency due to reduced light absorption (Figure 21.8c and d).

Li and the co-workers have reported heavy metal-free $CuInS_2$/ZnS core–shell QDs with a PLQY of 81% and large Stokes shift of 150 nm for the fabrication of LSCs, which exhibited an optical efficiency of 26.5%.[80] The $CuInS_2$/ZnS core–shell QDs were designed to absorb light of short wavelength (<450 nm) and re-emit as long wavelength light (~550 nm), which can be waveguided to the coupled crystalline-silicon (c-Si) PV cells. Such $CuInS_2$/ZnS core–shell QDs-LSC coupled PV device demonstrated an enhanced PCE of 8.71% compared to PV device without QDs-LSC (2.73%), *i.e.* Poly(methyl methacrylate) (PMMA) coupled PV device. The investigations related to QDs-based LSC infer that the cost of electricity production from PV cells can be reduced by employing QDs-based LSC technology.

21.4.4   Photodetectors

Photodetectors convert incident light into electrical signal and have attracted tremendous interest for their enormous applications in commercial and military fields.[81,82] Solution-processed device fabrication *via* colloidal QDs is an attractive approach to considerably lower the device fabrication cost.[83,84] In addition to the low fabrication cost, QDs also present size-dependent optical properties which can be utilized in photodetection to achieve diverse photodetection regimes.[85] However, compared to bare QDs, the core–shell QDs present improved photochemical stability and charge transfer characteristics due to the formation of type II or quasi-type II band structures which are vital for durable and high-performance photodetectors.[86] Chu's group has reported ZnCdSe/ZnS core–shell QDs-based photodetector fabricated on a thin layer of MoS_2.[87] The ZnCdSe/ZnS core–shell QDs act as light absorbers whereas the MoS_2 layer acts as the charge transporting channel. The schematic design of the ZnCdSe/ZnS core–shell QDs coupled with a MoS_2 layer-based photodetector is shown in Figure 21.9a. After illumination, the electron–hole pairs generated into QDs tunnel from QDs to MoS_2 channel and generate a photocurrent. Figure 21.9a shows QDs/MoS_2 photodetector device illuminated by incident wavelength of $\lambda = 450$ nm and $P = 400$ nW. The QDs/MoS_2 photodetector generated a considerably high photocurrent compared to only MoS_2-photodetector, as exhibited in Figure 21.9b.

Moreover, the ZnCdSe/ZnS core–shell QDs-based photodetector demonstrated faster rise/decay times as shown in Figure 21.9c and d which are ascribed to efficient injection of charge carrier from QDs to MoS_2 layer.[88]
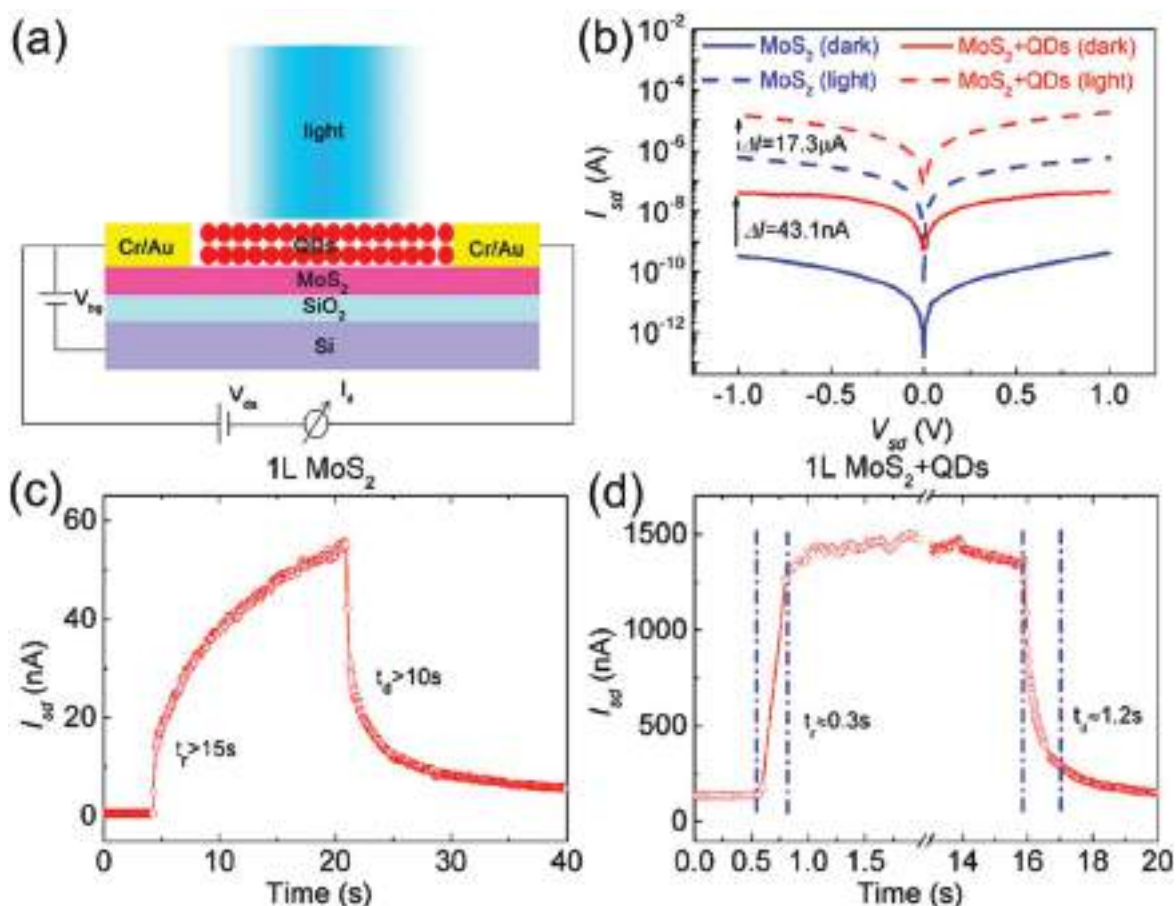
Figure 21.9 (a) Cross-sectional view of the schematic QDs/MoS_2 photodetector operated under illumination. (b) I–V curves of the MoS_2 photodetector device and QDs/MoS_2 hybrid device with and without 450 nm illumination keeping gate voltage (V_{bg}) = 0 V. (c, d) Time-dependent photoresponse of the pristine MoS_2 device and hybrid QD/MoS_2 devices. Adapted from ref. 87 with permission from American Chemical Society, Copyright 2019.

The faster rise/decay times are highly required for ultrafast responsive photodetectors and efficient carrier separation is the key to sensitive photodetectors.[89] The bare QDs are prone to the formation of charge trapping centers due to long term exposure in harsh environmental conditions which can lower the photodetector performance over time.[4,90] Moreover, the ZnCdSe/ZnS core–shell QDs-based photodetector exhibited much higher responsivity (~10^4 A W^{-1}) compared to photodetector without QDs (~10 A W^{-1}) and enhanced detectivity of 1.0×10^{12} Jones (about three orders of magnitude higher) compared to photodetector without QDs (4.6×10^9 Jones).[87]

21.4.5 Light Emitting Diodes

A light emitting diode (LED) is a device made up of semiconductors, which can emit light upon current injection. QDs-based LEDs (QLEDs) have gained much attention owing to their incredible features such as high brightness and color purity, low operating voltage and easy fabrication technologies.[91,92]

A QLED generally consists of a cathode, electron transport layer (ETL), QD layer for light emission, hole transport layer (HTL) and an anode as shown in Figure 21.10a.[93] Briefly, in QLEDs an external voltage is applied across the electrodes which causes the electrons and holes to transfer to ETL and HTL, respectively. The charges are then captured by QDs where they recombine and produce electroluminescence (EL).[94] Core–shell QDs have shown promising results for high-performance QLEDs owing to their higher photo-/chemical stability and PLQY.[95,96] Peng's group have developed red QLEDs employing CdSe/CdS core–shell QDs.[97] The CdSe/CdS core–shell QLED exhibited an external quantum efficiency (EQE) of 20.5% and a brightness of 1200 cd m^{-2}. However, by increasing the operating voltage up to 8 V the brightness can be reached as high as 42 000 cd m^{-2} with a simultaneous reduction in EQE. A similar decreasing trend in the EQE with increasing luminance was observed by Kazlas *et al.*[98] The performance of QLEDs is sensitive to the non-radiative Förster resonant energy transfer (FRET) process due to the closed packing of QDs, as a result of thin shell in core–shell QDs
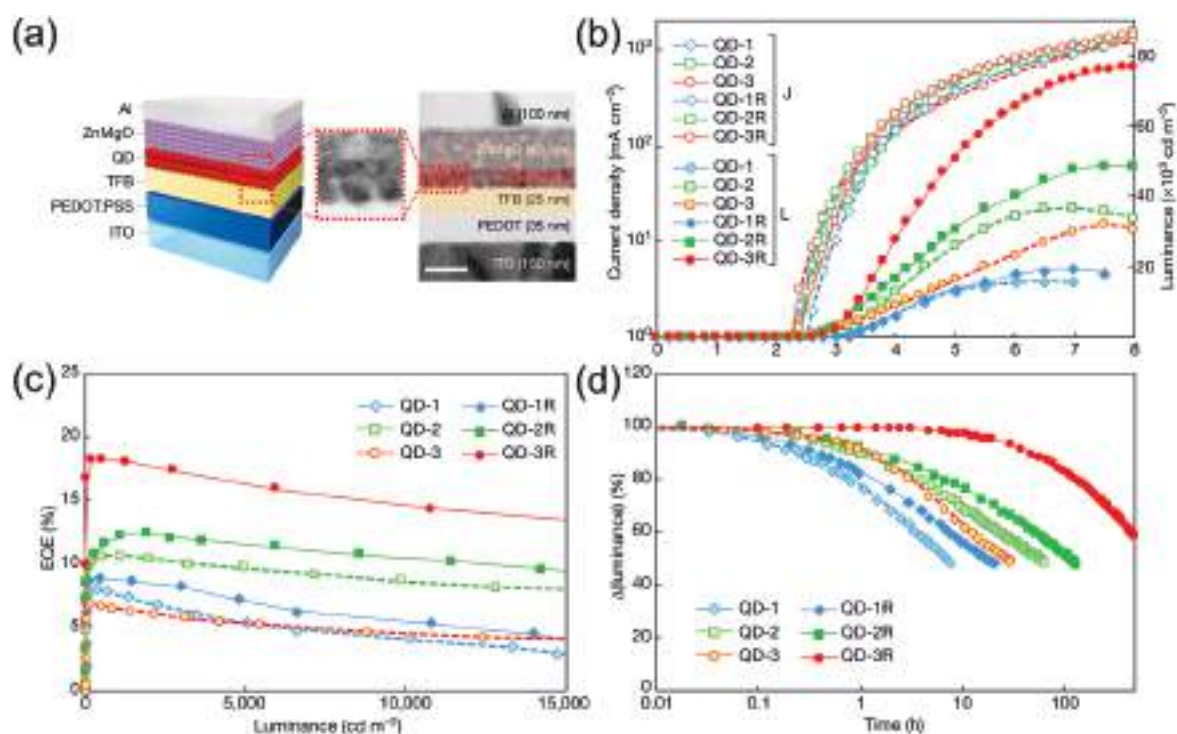

Figure 21.10   (a) Schematic illustration and cross-sectional TEM image of QLED device structure (scale bar, 50 nm). (b) Current density (left axis) and luminance (right axis) *versus* voltage profiles. (c) EQE-luminance profiles. (d) Lifetime measurements (at the initial luminance of 4500 cd m^{-2}) of the QLEDs with QD-1, QD-1R, QD-2, QD-2R, QD-3 and QD-3R. Note: QD-1, QD-2 and QD-3 refer to InP/ZnSe/ZnS (pod shaped) core/multi-shell QDs with variable ZnSe/ZnS shell thickness grown at 320 °C, whereas QD-1R, QD-2R and QD-3R represent InP/ZnSe/ZnS (spherical) core-multi-shell QDs with variable ZnSe/ZnS shell thickness grown at 340 °C. Adapted from ref. 106 with permission from Springer Nature, Copyright 2019.

and Auger recombination (AR).[99,100] Growth of thick multiple shells on core QDs has demonstrated a reduction of FRET and improved EQE compared to thin shell case.[101] Peng *et al.* optimized the performance of InP/ZnSe/ZnS core–shell–shell QDs-based LEDs to show an EQE of 12.2% and a brightness of over 10 000 cd m^{-2} by growing a thick shell and controlling the stoichiometry of the core–shell QDs.[102] The recent developments in QLED technologies have shown to exhibit either high EQE with low luminance or *vice versa*.[97,103–105] For instance, red light emitting CdSe/CdS core–shell QDs-based LEDs have reached an EQE in the range 18–20.5% with luminance limited in the range 100–2000 cd m^{-2}.[97,98]

Green QLEDs fabricated using CdSe/ZnS core–shell QDs have obtained high luminances of ~460 000 cd m^{-2} with EQE of 6%.[107] Blue QLEDs fabricated employing ZnCdS/ZnS core–shell QDs have reached an EQE of 10%, with a brightness of ~7600 cd m^{-2}.[108] Therefore, strategies are required to develop the enhancement of both EQE and the luminance of QLEDs.

Recently, Jang *et al.* have reported a tremendous improvement in the performance of red QLEDs by simultaneously enhancing both EQE and luminance.[106] They employed InP QDs over-coated by multiple thick shells of ZnSe and ZnS. However, prior to the shell growth on InP QDs, they performed surface treatment of InP core QDs during synthesis to alleviate the surface defects.[106] The surface treatment involved an *in situ* etching of InP core QDs for the removal of surface oxide which was conducted using hydrofluoric acid (HF). Multiple thick shells of ZnSe and ZnS were grown to eradicate non-radiative processes such as AR and FRET. However, the InP/ZnSe/ZnS core–shell/shell QDs obtained were observed to be pod shaped (termed QD-1, QD-2 and QD-3) with QYs of 98%, 92% and 75%, respectively. To obtain spherical shaped InP/ZnSe/ZnS core–shell–shell QDs (termed QD-1R, QD-2R and QD-3R) with enhanced QY (up to 100%) the shell growth temperature was increased to 340 °C. All the InP/ZnSe/ZnS core–shell–shell QDs-based LEDs exhibited a very low turn-on voltage in the range 1.8–2.0 V, which is close to the bandgap of InP QDs (~1.97 eV). The *I–V* curves for all the QLEDs devices with different ZnSe/ZnS shell thicknesses (both pod and spherical shaped) indicated identical charge transport as shown in Figure 21.10b. However, despite the similar transport behavior, the enhanced EQE and luminance was observed only for thicker ZnSe interlayer thicknesses (QD-3R). A maximum EQE of 18.0% and maximum luminance of 70 718 cd m^{-2} were observed for QLEDs fabricated from InP/ZnSe/ZnS (QD-3R, spherical shaped) core–shell–shell QDs with very thick ZnSe interlayer, as represented in Figure 21.10c. The QLED fabricated employing InP/ZnSe/ZnS QDs (QD-3, pod shaped) exhibited lower EQE and luminance due to its low PLQY (~75%) compared to the InP/ZnSe/ZnS (QD-3R, spherical shaped) core–shell–shell QDs. The low performance of InP/ZnSe/ZnS core-thin-shell QDs (both pod and spherical shaped) can be ascribed to the dominant FRET process.[106] In addition to the high-performance, the QLEDs with thicker ZnSe/ZnS shell (QD-3R, spherical shaped) demonstrated much enhanced durability compared to InP/ZnSe/ZnS core-thin-shell (both pod and spherical shaped) QDs-based LEDs, as shown in Figure 21.10d.

The QLED fabricated using InP/ZnSe/ZnS (QD-3R, spherical shaped) core//shell/shell QDs exhibited a remarkable predicted lifetime of about ~3000 h at a brightness of 1000 cd m^{-2}. The results infer that the spherical morphology of core–shell QDs with over-thick shells and much higher QY is promising for high-performance QLEDs.

21.4.6   Laser

In lasers, colloidal QDs have demonstrated advantageous features including tunable emission wavelength over a wide spectral range by the variation of QDs size with a low lasing threshold.[109] However, the bare QDs possess defects such as AR affecting the lifetime and bandwidth of optical gain and causes blinked emission from QDs, hindering the advanced development of QDs-based lasers.[110] Growth of thick shell on bare QDs can suppress the AR, making the core–shell QDs promising for laser application with continuous-wave operation and low-threshold amplification due to alleviated defects compared to bare QDs.[111–115]

Liao's group has reported the laser fabricated from a pure phase CdSe/CdS core–shell QDs and achieved single mode lasing with low thresholds of 16 μJ cm^{-2} and 2 μJ cm^{-2}.[112] These features were attributed to the suppressed AR in pure phase CdSe/CdS core–shell QDs. Dang *et al.* have reported type I CdSe/ZnCdS core–shell QDs with a PLQY of 80% for the fabrication of vertical-cavity surface-emitting lasers (VCSELs).[116] The schematic diagram of a VCSEL setup is shown in Figure 21.11a which is equipped with a long pass filter to wipe out residual pump excitation beam. Figure 21.11b shows pump energy dependent emission spectra, where sharp and coherent laser lines seem to appear above threshold energy. The lasing action triggered at a pumping threshold of ~60 μJ cm^{-2} for red light emitting laser. The QD-VCSEL exhibited an overall efficiency of 0.4% for red laser at an excitation energy density of 140 μJ cm^{-2}.
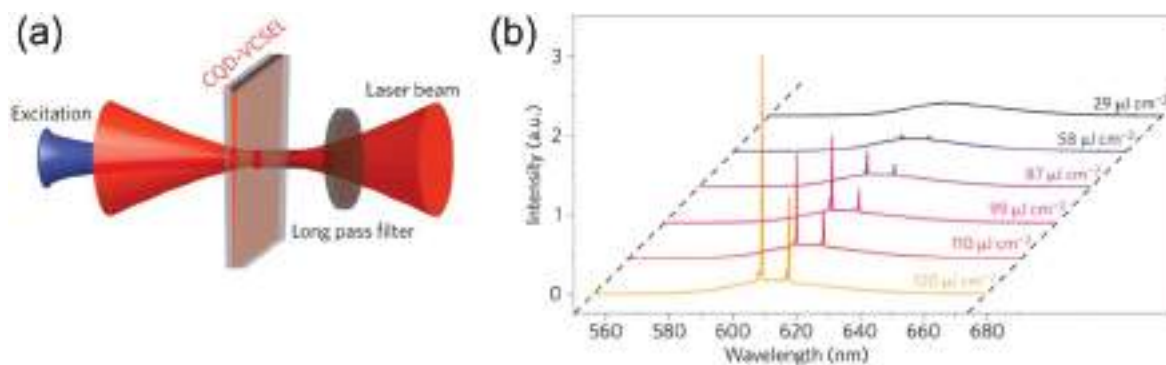

Figure 21.11   (a) Schematic diagram of a vertically pump CQD-VCSEL. (b) Emerging laser modes from spontaneous emission in a QD-VCSEL at increasing pump power. Adapted from ref. 116 with permission from Springer Nature, Copyright 2012.

Thick shell on QDs can further enable color switching in QDs-based lasers, *i.e.* the lasing can be switched from the core to shell.[117] Norris *et al.* have reported such color-tunable QDs-based lasers, they fabricated ring lasers with active color control *via* high-quality resonators through QD template stripping.[117] For lasing action, the as-fabricated QDs ring was illuminated by ultrafast laser pulses which demonstrated various features as a function of incident pulse energy: (i) Below the lasing threshold of 22 μJ cm^{-2}, only spontaneous emission was observed and a significant biexciton population can be expected to occur at an average exciton occupancy per QD $\langle N \rangle = 1.6$. (ii) Above the threshold energy, series of sharp laser peaks at a wavelength of ~610 nm appeared in the emission spectrum combined with ultrafast components (<100 ps) in the decay curve, which is the typical signature of stimulated emission. Further increase of excitation power resulted in the increased intensity of these laser peaks and the amplitude of the fast decay component followed by the beginning of red lasing, which saturated at around 80 μJ cm^{-2} ($\langle N \rangle = 5.9$). At 110 μJ cm^{-2} ($\langle N \rangle = 8.4$), the laser peaks switched to green lasing peaks emerging at 530 nm. (iii) Red lasing peaks and the fast decay components begin to diminish at higher pulse power. (iv) Finally, the green lasing peaks eventually grow stronger and dominate the device output.[117] These findings demonstrated that color switchable lasers can be fabricated by employing core–shell QDs as demonstrated by Norris and co-workers.

21.5 Conclusions

This chapter is dedicated to the chemical synthesis, optical properties and optoelectronic applications of various core–shell QDs. Recent progress for the development of different types of colloidal core–shell QDs (*e.g.*, type I, type II and quasi-type II) and their promising applications in light conversion (QDSCs, PEC cells and LSCs), light detection (photodetectors) and light emission (LEDs and lasers) have been presented. In particular, we highlighted the band alignment tuning *via* core–shell structures for achieving specific optoelectronic properties of QDs. It was revealed that the core–shell QDs with type II and quasi-type II band alignment are more beneficial to the PV applications owing to their intrinsic charge separation capability, while type I core–shell QDs with PLQY close to unity are the potential candidates for the light emitting devices. Moreover, the non-radiative process such as AR and FRET can be alleviated and charge-localization rates can be tuned by engineering the shell volume and the core–shell interface geometry, which can aid further development of QDs-based light emitting and PV devices.

To date, despite all the favorable conditions such as type II band alignment of core–shell QDs, which facilitates intrinsic charge separation and broad light absorption capabilities, the QDSCs suffer limited PCE and low V_{oc} values. In the case of QDs-based PEC cells, the PEC performance has covered a milestone, while the device stability is still a major problem owing to QDs degradation. Various strategies for improving device stability have been

employed and the obtained results showed that there is a trade-off between stability and performance. The LSC technology is a major breakthrough for low cost, high-performance building integrated PV devices, however, current QDs-based LSCs are prototypes with small dimensions. Besides the dimension issue, the PCEs of solar cells coupled with LSCs are still low. For ultrafast responsive photodetectors, the QDs-based photodetectors still require a major breakthrough to reach improved rise/decay time, responsivity and detectivity, which are dependent on the efficient charge extraction from the QDs and their transport properties. For QLEDs and lasers, the device performance is greatly affected by the non-radiative phenomena such as AR and FRET processes owing to the large surface area of QDs.

Besides, the major issue among state-of-the-art QDs-based optoelectronic devices is the use of QDs with heavy metals (such as Pb, Cd *etc.*), which are harmful to the environment and human health and hinder their practical usages. Therefore, it is suggested that developing heavy metal-free core–shell QDs (typically, I-III-VI group QDs) with excellent optical properties are essential and promising for prospective high-performance QDs-based optoelectronics. Unfortunately, due to their complex optical properties (*e.g.*, defect-related emission), current heavy metal-free core–shell QDs-based solar energy conversion devices suffer lower performance challenges despite their intrinsic broad light absorption as compared to heavy metals-based core–shell QDs. More effective approaches for enhancing the optical properties of heavy metal-free core–shell QDs and optimizing the performance of corresponding QD-devices should be explored in terms of future commercialization.

References

1. G. H. Carey, A. L. Abdelhady, Z. Ning, S. M. Thon, O. M. Bakr and E. H. Sargent, *Chem. Rev.*, 2015, **115**, 12732.
2. R. Ghosh Chaudhuri and S. Paria, *Chem. Rev.*, 2012, **112**, 2373.
3. A. M. Smith and S. Nie, *Acc. Chem. Res.*, 2010, **43**, 190.
4. H. Zhao and F. Rosei, *Chem*, 2017, **3**, 229.
5. C. Giansante and I. Infante, *J. Phys. Chem. Lett.*, 2017, **8**, 5209.
6. H. Moon, C. Lee, W. Lee, J. Kim and H. Chae, *Adv. Mater.*, 2019, **31**, 1804294.
7. C. B. Murray, C. R. Kagan and M. G. Bawendi, *Science*, 1995, **270**, 1335.
8. M. Green, *J. Mater. Chem.*, 2010, **20**, 5797.
9. A. I. Channa, X. Tong, J.-Y. Xu, Y. Liu, C. Wang, M. N. Sial, P. Yu, H. Ji, X. Niu and Z. M. Wang, *J. Mater. Chem. A*, 2019, **7**, 10225.
10. A. Piryatinski, S. A. Ivanov, S. Tretiak and V. I. Klimov, *Nano Lett.*, 2007, **7**, 108.
11. S. Kim, B. Fisher, H.-J. Eisler and M. Bawendi, *J. Am. Chem. Soc.*, 2003, **125**, 11466.
12. H. Zhu, N. Song and T. Lian, *J. Am. Chem. Soc.*, 2011, **133**, 8762.

13. Y. Jia, J. Chen, K. Wu, A. Kaledin, D. G. Musaev, Z. Xie and T. Lian, *Chem. Sci.*, 2016, **7**, 4125.
14. M. Jalalah, M. S. Al-Assiri and J.-G. Park, *Adv. Energy Mater.*, 2018, **8**, 1703418.
15. J. S. Steckel, J. P. Zimmer, S. Coe-Sullivan, N. E. Stott, V. Bulović and M. G. Bawendi, *Angew. Chem., Int. Ed.*, 2004, **43**, 2154.
16. L. Li and P. Reiss, *J. Am. Chem. Soc.*, 2008, **130**, 11588.
17. J. B. Sambur and B. A. Parkinson, *J. Am. Chem. Soc.*, 2010, **132**, 2130.
18. M. A. Hines and P. Guyot-Sionnest, *J. Phys. Chem.*, 1996, **100**, 468.
19. J.-J. Hao, J. Zhou and C.-Y. Zhang, *Chem. Commun.*, 2013, **49**, 6346.
20. B. Chon, S. J. Lim, W. Kim, J. Seo, H. Kang, T. Joo, J. Hwang and S. K. Shin, *Phys. Chem. Chem. Phys.*, 2010, **12**, 9312.
21. B. Dong, L. Cao, G. Su and W. Liu, *Chem. Commun.*, 2010, **46**, 7331.
22. B. O. Dabbousi, J. Rodriguez-Viejo, F. V. Mikulec, J. R. Heine, H. Mattoussi, R. Ober, K. F. Jensen and M. G. Bawendi, *J. Phys. Chem. B*, 1997, **101**, 9463.
23. D. V. Talapin, A. L. Rogach, A. Kornowski, M. Haase and H. Weller, *Nano Lett.*, 2001, **1**, 207.
24. S. Kudera, M. Zanella, C. Giannini, A. Rizzo, Y. Li, G. Gigli, R. Cingolani, G. Ciccarella, W. Spahl, W. J. Parak and L. Manna, *Adv. Mater.*, 2007, **19**, 548.
25. H. Zhu, N. Song and T. Lian, *J. Am. Chem. Soc.*, 2010, **132**, 15038.
26. K. Yu, B. Zaman, S. Romanova, D.-s. Wang and J. A. Ripmeester, *Small*, 2005, **1**, 332.
27. J. Wang, I. Mora-Seró, Z. Pan, K. Zhao, H. Zhang, Y. Feng, G. Yang, X. Zhong and J. Bisquert, *J. Am. Chem. Soc.*, 2013, **135**, 15913.
28. R. Xie, X. Zhong and T. Basché, *Adv. Mater.*, 2005, **17**, 2741.
29. R. Xie, U. Kolb and T. Basché, *Small*, 2006, **2**, 1454.
30. D. J. Milliron, S. M. Hughes, Y. Cui, L. Manna, J. Li, L.-W. Wang and A. Paul Alivisatos, *Nature*, 2004, **430**, 190.
31. S. A. Ivanov, A. Piryatinski, J. Nanda, S. Tretiak, K. R. Zavadil, W. O. Wallace, D. Werder and V. I. Klimov, *J. Am. Chem. Soc.*, 2007, **129**, 11708.
32. A. M. Smith, A. M. Mohs and S. Nie, *Nat. Nanotechnol.*, 2009, **4**, 56.
33. J. Bang, J. Park, J. H. Lee, N. Won, J. Nam, J. Lim, B. Y. Chang, H. J. Lee, B. Chon, J. Shin, J. B. Park, J. H. Choi, K. Cho, S. M. Park, T. Joo and S. Kim, *Chem. Mater.*, 2010, **22**, 233.
34. S. Kim, Y. T. Lim, E. G. Soltesz, A. M. De Grand, J. Lee, A. Nakayama, J. A. Parker, T. Mihaljevic, R. G. Laurence, D. M. Dor, L. H. Cohn, M. G. Bawendi and J. V. Frangioni, *Nat. Biotechnol.*, 2004, **22**, 93.
35. X. Tong, X. Li, A. I. Channa, R. Liu, J.-Y. Xu, P. Yu, L. Chang, H. Ji, Q. Wang and Z. M. Wang, *Sol. RRL*, 2019, **3**, 1900186.
36. C.-Y. Chen, C.-T. Cheng, J.-K. Yu, S.-C. Pu, Y.-M. Cheng, P.-T. Chou, Y.-H. Chou and H.-T. Chiu, *J. Phys. Chem. B*, 2004, **108**, 10687.
37. N. N. Hewa-Kasakarage, M. Kirsanova, A. Nemchinov, N. Schmall, P. Z. El-Khoury, A. N. Tarnovsky and M. Zamkov, *J. Am. Chem. Soc.*, 2009, **131**, 1328.

38. S. Brovelli, R. D. Schaller, S. A. Crooker, F. García-Santamaría, Y. Chen, R. Viswanatha, J. A. Hollingsworth, H. Htoon and V. I. Klimov, *Nat. Commun.*, 2011, **2**, 280.

39. C. Wang, X. Tong, W. Wang, J.-Y. Xu, L. V. Besteiro, A. I. Channa, F. Lin, J. Wu, Q. Wang, A. O. Govorov, A. Vomiero and Z. M. Wang, *ACS Appl. Mater. Interfaces*, 2020, **12**, 36277.

40. K. Wu, N. Song, Z. Liu, H. Zhu, W. Rodríguez-Córdoba and T. Lian, *J. Phys. Chem. A*, 2013, **117**, 7561.

41. F. García-Santamaría, S. Brovelli, R. Viswanatha, J. A. Hollingsworth, H. Htoon, S. A. Crooker and V. I. Klimov, *Nano Lett.*, 2011, **11**, 687.

42. A. Pandey and P. Guyot-Sionnest, *Science*, 2008, **322**, 929.

43. B. De Geyter, Y. Justo, I. Moreels, K. Lambert, P. F. Smet, D. Van Thourhout, A. J. Houtepen, D. Grodzinska, C. de Mello Donega, A. Meijerink, D. Vanmaekelbergh and Z. Hens, *ACS Nano*, 2011, **5**, 58.

44. X. Tong, X.-T. Kong, Y. Zhou, F. Navarro-Pardo, G. S. Selopal, S. Sun, A. O. Govorov, H. Zhao, Z. M. Wang and F. Rosei, *Adv. Energy Mater.*, 2018, **8**, 1701432.

45. X. Tong, X.-T. Kong, C. Wang, Y. Zhou, F. Navarro-Pardo, D. Barba, D. Ma, S. Sun, A. O. Govorov, H. Zhao, Z. M. Wang and F. Rosei, *Adv. Sci.*, 2018, **5**, 1800656.

46. X. Wen, A. Sitt, P. Yu, Y.-R. Toh and J. Tang, *Phys. Chem. Chem. Phys.*, 2012, **14**, 3505.

47. B. N. Pal, Y. Ghosh, S. Brovelli, R. Laocharoensuk, V. I. Klimov, J. A. Hollingsworth and H. Htoon, *Nano Lett.*, 2012, **12**, 331.

48. D. Kong, Y. Jia, Y. Ren, Z. Xie, K. Wu and T. Lian, *J. Phys. Chem. C*, 2018, **122**, 14091.

49. D. Yu, C. Wang and P. Guyot-Sionnest, *Science*, 2003, **300**, 1277.

50. H. Zhu, N. Song, W. Rodríguez-Córdoba and T. Lian, *J. Am. Chem. Soc.*, 2012, **134**, 4250.

51. Z. Pan, H. Rao, I. Mora-Seró, J. Bisquert and X. Zhong, *Chem. Soc. Rev.*, 2018, **47**, 7659.

52. S. Jiao, Q. Shen, I. Mora-Seró, J. Wang, Z. Pan, K. Zhao, Y. Kuga, X. Zhong and J. Bisquert, *ACS Nano*, 2015, **9**, 908.

53. Z. Ning, H. Tian, C. Yuan, Y. Fu, H. Qin, L. Sun and H. Ågren, *Chem. Commun.*, 2011, **47**, 1536.

54. J. Yang and X. Zhong, *J. Mater. Chem. A*, 2016, **4**, 16553–16561.

55. J. Luo, H. Wei, F. Li, Q. Huang, D. Li, Y. Luo and Q. Meng, *Chem. Commun.*, 2014, **50**, 3464.

56. J. Yang, J. Wang, K. Zhao, T. Izuishi, Y. Li, Q. Shen and X. Zhong, *J. Phys. Chem. C*, 2015, **119**, 28800–28808.

57. S. Buhbut, S. Itzhakov, I. Hod, D. Oron and A. Zaban, *Nano Lett.*, 2013, **13**, 4456.

58. M. Kazes, S. Buhbut, S. Itzhakov, O. Lahad, A. Zaban and D. Oron, *J. Phys. Chem. Lett.*, 2014, **5**, 2717.

59. S. Sahai, A. Ikram, S. Rai, R. Shrivastav, S. Dass and V. R. Satsangi, *Renewable Sustainable Energy Rev.*, 2017, **68**, 19.

60. L. Jin, B. AlOtaibi, D. Benetti, S. Li, H. Zhao, Z. Mi, A. Vomiero and F. Rosei, *Adv. Sci.*, 2016, **3**, 1500345.
61. K. Wang, X. Tong, Y. Zhou, H. Zhang, F. Navarro-Pardo, G. S. Selopal, G. Liu, J. Tang, Y. Wang, S. Sun, D. Ma, Z. M. Wang, F. Vidal, H. Zhao, X. Sun and F. Rosei, *J. Mater. Chem. A*, 2019, **7**, 14079.
62. R. Wang, X. Tong, A. I. Channa, Q. Zeng, J. Sun, C. Liu, X. Li, J. Xu, F. Lin, G. S. Selopal, F. Rosei, Y. Zhang, J. Wu, H. Zhao, A. Vomiero, X. Sun and Z. M. Wang, *J. Mater. Chem. A*, 2020, **8**, 10736.
63. X. Tong, Y. Zhou, L. Jin, K. Basu, R. Adhikari, G. S. Selopal, X. Tong, H. Zhao, S. Sun, A. Vomiero, Z. M. Wang and F. Rosei, *Nano Energy*, 2017, **31**, 441.
64. N. D. Bronstein, Y. Yao, L. Xu, E. O'Brien, A. S. Powers, V. E. Ferry, A. P. Alivisatos and R. G. Nuzzo, *ACS Photonics*, 2015, **2**, 1576–1583.
65. Y. You, X. Tong, W. Wang, J. Sun, P. Yu, H. Ji, X. Niu and Z. M. Wang, *Adv. Sci.*, 2019, **6**, 1801967.
66. F. Purcell-Milton and Y. K. Gun'ko, *J. Mater. Chem.*, 2012, **22**, 16687.
67. K. Wu, H. Li and V. I. Klimov, *Nat. Photonics*, 2018, **12**, 105.
68. Y. Zhou, H. Zhao, D. Ma and F. Rosei, *Chem. Soc. Rev.*, 2018, **47**, 5866.
69. S. Sadeghi, H. Bahmani Jalali, R. Melikov, B. Ganesh Kumar, M. Mohammadi Aria, C. W. Ow-Yang and S. Nizamoglu, *ACS Appl. Mater. Interfaces*, 2018, **10**, 12975.
70. M. Sharma, K. Gungor, A. Yeltik, M. Olutas, B. Guzelturk, Y. Kelestemur, T. Erdem, S. Delikanli, J. R. McBride and H. V. Demir, *Adv. Mater.*, 2017, **29**, 1700821.
71. H. Zhao, D. Benetti, L. Jin, Y. Zhou, F. Rosei and A. Vomiero, *Small*, 2016, **12**, 5354.
72. M. J. Currie, J. K. Mapel, T. D. Heidel, S. Goffri and M. A. Baldo, *Science*, 2008, **321**, 226.
73. R. Mazzaro and A. Vomiero, *Adv. Energy Mater.*, 2018, **8**, 1801903.
74. U. Resch-Genger, M. Grabolle, S. Cavaliere-Jaricot, R. Nitschke and T. Nann, *Nat. Methods*, 2008, **5**, 763.
75. L. Xu, Y. Yao, N. D. Bronstein, L. Li, A. P. Alivisatos and R. G. Nuzzo, *ACS Photonics*, 2016, **3**, 278.
76. F. Meinardi, A. Colombo, K. A. Velizhanin, R. Simonutti, M. Lorenzon, L. Beverina, R. Viswanatha, V. I. Klimov and S. Brovelli, *Nat. Photonics*, 2014, **8**, 392.
77. Y. Zhou, D. Benetti, Z. Fan, H. Zhao, D. Ma, A. O. Govorov, A. Vomiero and F. Rosei, *Adv. Energy Mater.*, 2016, **6**, 1501913.
78. H. Zhao, M. Chaker and D. Ma, *J. Mater. Chem.*, 2011, **21**, 17483.
79. I. Coropceanu and M. G. Bawendi, *Nano Lett.*, 2014, **14**, 4097.
80. C. Li, W. Chen, D. Wu, D. Quan, Z. Zhou, J. Hao, J. Qin, Y. Li, Z. He and K. Wang, *Sci. Rep.*, 2015, **5**, 17777.
81. L. Peng, L. Hu and X. Fang, *Adv. Mater.*, 2013, **25**, 5321.
82. S. Liu, M.-Y. Li, D. Su, M. Yu, H. Kan, H. Liu, X. Wang and S. Jiang, *ACS Appl. Mater. Interfaces*, 2018, **10**, 32516.

83. G. Konstantatos, I. Howard, A. Fischer, S. Hoogland, J. Clifford, E. Klem, L. Levina and E. H. Sargent, *Nature*, 2006, **442**, 180.

84. S. A. McDonald, G. Konstantatos, S. Zhang, P. W. Cyr, E. J. D. Klem, L. Levina and E. H. Sargent, *Nat. Mater.*, 2005, **4**, 138.

85. L. Gao, C. Chen, K. Zeng, C. Ge, D. Yang, H. Song and J. Tang, *Light: Sci. Appl.*, 2016, **5**, e16126.

86. W. Ouyang, F. Teng, J.-H. He and X. Fang, *Adv. Funct. Mater.*, 2019, **29**, 1807672.

87. S. Zhang, X. Wang, Y. Chen, G. Wu, Y. Tang, L. Zhu, H. Wang, W. Jiang, L. Sun, T. Lin, H. Shen, W. Hu, J. Ge, J. Wang, X. Meng and J. Chu, *ACS Appl. Mater. Interfaces*, 2019, **11**, 23667.

88. Y.-H. Chang, W. Zhang, Y. Zhu, Y. Han, J. Pu, J.-K. Chang, W.-T. Hsu, J.-K. Huang, C.-L. Hsu, M.-H. Chiu, T. Takenobu, H. Li, C.-I. Wu, W.-H. Chang, A. T. S. Wee and L.-J. Li, *ACS Nano*, 2014, **8**, 8582.

89. S. Pak, Y. Cho, J. Hong, J. Lee, S. Lee, B. Hou, G.-H. An, Y.-W. Lee, J. E. Jang, H. Im, S. M. Morris, J. I. Sohn, S. Cha and J. M. Kim, *ACS Appl. Mater. Interfaces*, 2018, **10**, 38264–38271.

90. C. Bi, S. V. Kershaw, A. L. Rogach and J. Tian, *Adv. Funct. Mater.*, 2019, **29**, 1902446.

91. X. Dai, Y. Deng, X. Peng and Y. Jin, *Adv. Mater.*, 2017, **29**, 1607022.

92. S. Pimputkar, J. S. Speck, S. P. DenBaars and S. Nakamura, *Nat. Photonics*, 2009, **3**, 180.

93. P. O. Anikeeva, J. E. Halpert, M. G. Bawendi and V. Bulović, *Nano Lett.*, 2009, **9**, 2532.

94. Z. Yang, M. Gao, W. Wu, X. Yang, X. W. Sun, J. Zhang, H.-C. Wang, R.-S. Liu, C.-Y. Han, H. Yang and W. Li, *Mater. Today*, 2019, **24**, 69.

95. Y.-C. Pu and Y.-J. Hsu, *Nanoscale*, 2014, **6**, 3881.

96. J. Lim, B. G. Jeong, M. Park, J. K. Kim, J. M. Pietryga, Y.-S. Park, V. I. Klimov, C. Lee, D. C. Lee and W. K. Bae, *Adv. Mater.*, 2014, **26**, 8034.

97. X. Dai, Z. Zhang, Y. Jin, Y. Niu, H. Cao, X. Liang, L. Chen, J. Wang and X. Peng, *Nature*, 2014, **515**, 96.

98. B. S. Mashford, M. Stevenson, Z. Popovic, C. Hamilton, Z. Zhou, C. Breen, J. Steckel, V. Bulovic, M. Bawendi, S. Coe-Sullivan and P. T. Kazlas, *Nat. Photonics*, 2013, **7**, 407.

99. D. Bozyigit, O. Yarema and V. Wood, *Adv. Funct. Mater.*, 2013, **23**, 3024.

100. Y. Shirasaki, G. J. Supran, W. A. Tisdale and V. Bulović, *Phys. Rev. Lett.*, 2013, **110**, 217403.

101. H. Zhang, N. Hu, Z. Zeng, Q. Lin, F. Zhang, A. Tang, Y. Jia, L. S. Li, H. Shen, F. Teng and Z. Du, *Adv. Opt. Mater.*, 2019, **7**, 1801602.

102. Y. Li, X. Hou, X. Dai, Z. Yao, L. Lv, Y. Jin and X. Peng, *J. Am. Chem. Soc.*, 2019, **141**, 6448.

103. H. Zhang, S. Chen and X. W. Sun, *ACS Nano*, 2018, **12**, 697–704.

104. Y. Shirasaki, G. J. Supran, M. G. Bawendi and V. Bulović, *Nat. Photonics*, 2013, **7**, 13.

105. H. Shen, Q. Gao, Y. Zhang, Y. Lin, Q. Lin, Z. Li, L. Chen, Z. Zeng, X. Li, Y. Jia, S. Wang, Z. Du, L. S. Li and Z. Zhang, *Nat. Photonics*, 2019, **13**, 192.

106. Y.-H. Won, O. Cho, T. Kim, D.-Y. Chung, T. Kim, H. Chung, H. Jang, J. Lee, D. Kim and E. Jang, *Nature*, 2019, **575**, 634.

107. X. Li, Y.-B. Zhao, F. Fan, L. Levina, M. Liu, R. Quintero-Bermudez, X. Gong, L. N. Quan, J. Fan, Z. Yang, S. Hoogland, O. Voznyy, Z.-H. Lu and E. H. Sargent, *Nat. Photonics*, 2018, **12**, 159.

108. H. Shen, W. Cao, N. T. Shewmon, C. Yang, L. S. Li and J. Xue, *Nano Lett.*, 2015, **15**, 1211.

109. V. I. Klimov, A. A. Mikhailovsky, S. Xu, A. Malko, J. A. Hollingsworth, C. A. Leatherdale, H. J. Eisler and M. G. Bawendi, *Science*, 2000, **290**, 314.

110. V. I. Klimov, A. A. Mikhailovsky, D. W. McBranch, C. A. Leatherdale and M. G. Bawendi, *Science*, 2000, **287**, 1011.

111. F. Fan, O. Voznyy, R. P. Sabatini, K. T. Bicanic, M. M. Adachi, J. R. McBride, K. R. Reid, Y.-S. Park, X. Li, A. Jain, R. Quintero-Bermudez, M. Saravana-pavanantham, M. Liu, M. Korkusinski, P. Hawrylak, V. I. Klimov, S. J. Rosenthal, S. Hoogland and E. H. Sargent, *Nature*, 2017, **544**, 75.

112. C. Liao, R. Xu, Y. Xu, C. Zhang, M. Xiao, L. Zhang, C. Lu, Y. Cui and J. Zhang, *J. Phys. Chem. Lett.*, 2016, **7**, 4968.

113. Y.-S. Park, W. K. Bae, T. Baker, J. Lim and V. I. Klimov, *Nano Lett.*, 2015, **15**, 7319.

114. M. Zavelani-Rossi, M. G. Lupo, R. Krahne, L. Manna and G. Lanzani, *Nanoscale*, 2010, **2**, 931.

115. F. García-Santamaría, Y. Chen, J. Vela, R. D. Schaller, J. A. Hollingsworth and V. I. Klimov, *Nano Lett.*, 2009, **9**, 3482.

116. C. Dang, J. Lee, C. Breen, J. S. Steckel, S. Coe-Sullivan and A. Nurmikko, *Nat. Nanotechnol.*, 2012, **7**, 335.

117. B. le Feber, F. Prins, E. De Leo, F. T. Rabouw and D. J. Norris, *Nano Lett.*, 2018, **18**, 1028.